Weak lensing tomography with orthogonal polynomials

Björn Malte Schäfer[1]★ and Lavinia Heisenberg[2]

[1]*Astronomisches Recheninstitut, Zentrum für Astronomie, Universität Heidelberg, Mönchhofstraße 12, 69120 Heidelberg, Germany*
[2]*Centre for Astroparticle Physics, Département de Physique Théorique, Université de Genève, 24 quai Ernest Ansermet, 1211 Genève, Switzerland*

ABSTRACT

The topic of this paper is weak cosmic shear tomography where the line-of-sight weighting is carried out with a set of specifically constructed orthogonal polynomials, dubbed Tomography with Orthogonal Radial Distance Polynomial Systems (TaRDiS). We investigate the properties of these polynomials and employ weak convergence spectra, which have been obtained by weighting with these polynomials, for the estimation of cosmological parameters. We quantify their power in constraining parameters in a Fisher matrix technique and demonstrate how each polynomial projects out statistically independent information, and how the combination of multiple polynomials lifts degeneracies. The assumption of a reference cosmology is needed for the construction of the polynomials, and as a last point we investigate how errors in the construction with a wrong cosmological model propagate to misestimates in cosmological parameters. TaRDiS performs on a similar level as traditional tomographic methods and some key features of tomography are made easier to understand.

Key words: gravitational lensing: weak – methods: analytical – large-scale structure of Universe.

1 INTRODUCTION

Weak gravitational lensing by the cosmic large-scale structure (Blandford et al. 1991; Schneider, Ehlers & Falco 1992; Seitz & Schneider 1994; Seitz, Schneider & Ehlers 1994; Kamionkowski et al. 1998) is regarded as a very promising way for investigating the properties of the cosmic matter distribution and the measurement of cosmological parameters. The primary tool is the angular spectra of the weak lensing convergence (Jain & Seljak 1997; Hu & Tegmark 1999; Hu & White 2001; Hu & Jain 2004), which has, in the context of dark energy cosmologies with adiabatic fluctuations in the dark matter distribution, the potential to deliver parameter constraints competitive with those from the cosmic microwave background (CMB).

The weak cosmic shearing effect of the large-scale structure has been detected by four independent research groups a decade ago (Bacon, Refregier & Ellis 2000; Kaiser, Wilson & Luppino 2000; Van Waerbeke et al. 2000; Wittman et al. 2000) and now parameter constraints derived from weak lensing spectra coincide well with those from the CMB, with a small tension concerning the parameters Ω_m and σ_8 (Kilbinger et al. 2009, 2010). These topics are reviewed in detail by Bartelmann & Schneider (2001) and Bartelmann (2010a,b).

Together with the property of weak lensing to map out fluctuations in the cosmic matter distribution in a linear way, tomographic

methods have been shown to offer superior precision in the determination of cosmological parameters (Hu 1999, 2002a,b; Takada & White 2004; Hannestad, Tu & Wong 2006), in particular concerning the properties of dark energy (Huterer & Turner 2001; Huterer 2002, 2010; Hollenstein et al. 2009; Amara & Kitching 2011; Lee 2011). The idea of tomography is a division of the galaxy sample used for shear estimation into a number of bins in distance. This splitting is the reason for two important advantages of tomography: the weak lensing convergence is a line-of-sight-integrated quantity of which one measures the angular fluctuation statistics. Angular convergence spectra, however, convey less information compared to the fluctuations statistics of the three-dimensional matter distribution because in the projection process, a mixing of scales is taking place. Secondly, cosmological parameters can have different influences on the amplitude of the weak lensing convergence at different redshifts, which would be averaged out. Combining convergence spectra measured for each subset of galaxies is able to alleviate these two problems. Related developments include shear ratio measurements, where the same tidal fields are measured with galaxy populations at different redshifts (Jain & Taylor 2003; Taylor et al. 2007), cross-correlation cosmography, where part of the galaxies is used for constructing a template on which one observes the shearing effect of more distant galaxies (Bernstein & Jain 2004), and finally three-dimensional weak shear methods, which provide a direct reconstruction of the fluctuations of the cosmic density field (Castro, Heavens & Kitching 2005; Heavens, Kitching & Taylor 2006; Kitching, Heavens & Miller 2011). Common to these methods are non-zero covariances between measurements of different

★E-mail: bjoern.malte.schaefer@uni-heidelberg.de

redshifts. This is a natural consequence that lensing is caused by the large-scale structure between the lensed objects and the observer, so that the light from different galaxy samples has to transverse partially the same large-scale structure for reaching the observer.

Our motivation is to revisit weak lensing tomography and to construct a weighing scheme for the galaxies as a function on distance, such that the covariances between spectra estimated from differently weighted galaxy samples have a particular simple, diagonal shape. For this goal, we construct a set of orthogonal polynomials in distance, which provides a diagonalization of the covariance, and which, when employed in the derivation of the convergence spectrum, projects out statistically independent information about the large-scale structure.

After a brief summary of key formulae for cosmology, structure formation and weak lensing in Section 2, we describe the construction of TaRDiS polynomials and investigate their properties in Section 3. Their statistical and systematical errors are evaluated in Sections 4 and 5, respectively, and we summarize our results in Section 6. The reference cosmological model used is a spatially flat w cold dark matter (wCDM) cosmology with Gaussian adiabatic initial perturbations in the CDM density field. The specific parameter choices are $\Omega_m = 0.25$, $\sigma_8 = 0.8$, $H_0 = 100\,h\,\mathrm{km\,s^{-1}\,Mpc^{-1}}$, with $h = 0.72$, $n_s = 1$ and $\Omega_b = 0.04$. The dark energy equation of state is set to $w = -0.9$ and the sound speed is equal to the speed of light ($c_s = c$) such that there is no clustering in the dark energy fluid.

2 COSMOLOGY AND WEAK LENSING

2.1 Dark energy cosmologies

In spatially flat dark energy cosmologies with the matter density parameter Ω_m, the Hubble function $H(a) = \mathrm{d}\ln a/\mathrm{d}t$ is given by

$$\frac{H^2(a)}{H_0^2} = \frac{\Omega_m}{a^3} + (1 - \Omega_m)\exp\left(3\int_a^1 \mathrm{d}\ln a\,[1 + w(a)]\right), \quad (1)$$

with the dark energy equation of state $w(a)$, for which we use the common parametrization (Chevallier & Polarski 2001):

$$w(a) = w_0 + (1 - a)w_a, \quad (2)$$

where $w_0 = -1$ and $w_a = 0$ would correspond to ΛCDM. Comoving distance χ and scale factor a are related by

$$\chi = c\int_a^1 \frac{\mathrm{d}a}{a^2 H(a)}, \quad (3)$$

such that the comoving distance is given in units of the Hubble distance $\chi_H = c/H_0$.

2.2 CDM power spectrum

The linear CDM density power spectrum $P(k)$ describes statistically homogeneous Gaussian fluctuations of the density field δ,

$$\langle\delta(\boldsymbol{k})\delta(\boldsymbol{k}')^*\rangle = (2\pi)^3\delta_D(\boldsymbol{k} - \boldsymbol{k}')P(k). \quad (4)$$

It is composed from a scale invariant term $\propto k^{n_s}$ and the transfer function $T(k)$,

$$P(k) \propto k^{n_s}T^2(k). \quad (5)$$

In low-Ω_m cosmologies $T(k)$ is approximated with the fit proposed by Bardeen et al. (1986):

$$T(q) = \frac{\ln(1 + 2.34q)}{2.34q}$$
$$\times\left(1 + 3.89q + (16.1q)^2 + (5.46q)^3 + (6.71q)^4\right)^{-(1/4)}, \quad (6)$$

where the wave vector $k = q\Gamma$ is given in units of the shape parameter Γ. Γ determines the peak shape of the CDM spectrum and is to first order given by $\Gamma = \Omega_m h$, with small corrections due to the baryon density Ω_b (Sugiyama 1995),

$$\Gamma = \Omega_m h\exp\left(-\Omega_b\left(1 + \frac{\sqrt{2h}}{\Omega_m}\right)\right). \quad (7)$$

The spectrum $P(k)$ is normalized to the variance σ_8 on the scale $R = 8\,\mathrm{Mpc}\,h^{-1}$,

$$\sigma_R^2 = \int \frac{\mathrm{d}\ln k}{2\pi^2}\,k^3 P(k)W_R^2(k), \quad (8)$$

with a Fourier transformed spherical top hat filter function, $W_R(k) = 3j_1(kR)/(kR)$. $j_\ell(x)$ is the spherical Bessel function of the first kind of order ℓ (Abramowitz & Stegun 1972).

2.3 Structure growth with clustering dark energy

Linear homogeneous growth of the density field, $\delta(\boldsymbol{x}, a) = D_+(a)\delta(\boldsymbol{x}, a = 1)$, is described by the growth function $D_+(a)$, which is the solution to the growth equation (Turner & White 1997; Wang & Steinhardt 1998; Linder & Jenkins 2003),

$$\frac{\mathrm{d}^2}{\mathrm{d}a^2}D_+(a) + \frac{1}{a}\left(3 + \frac{\mathrm{d}\ln H}{\mathrm{d}\ln a}\right)\frac{\mathrm{d}}{\mathrm{d}a}D_+(a) = \frac{3}{2a^2}\Omega_m(a)D_+(a). \quad (9)$$

Non-linear structure formation enhances the CDM spectrum $P(k)$ on small scales by a factor of $\simeq 40$, which is described by the fit suggested by Smith et al. (2003) which is gauged to n-body simulations of cosmic structure formation.

2.4 Weak gravitational lensing

The weak lensing convergence κ provides a weighted line-of-sight average of the matter density δ (for reviews, see Bartelmann & Schneider 2001; Bartelmann 2010b):

$$\kappa = \int_0^{\chi_H} \mathrm{d}\chi\,W_\kappa(\chi)\delta, \quad (10)$$

with the weak lensing efficiency $W_\kappa(\chi)$ as the weighting function,

$$W_\kappa(\chi) = \frac{3\Omega_m}{2\chi_H^2}\frac{D_+}{a}G(\chi)\chi, \text{ with } G(\chi) = \int_\chi^{\chi_H}\mathrm{d}\chi'\,n(z)\frac{\mathrm{d}z}{\mathrm{d}\chi'}\frac{\chi' - \chi}{\chi'}. \quad (11)$$

$n(z)$ denotes the redshift distribution of the lensed background galaxies,

$$n(z) = n_0\left(\frac{z}{z_0}\right)^2\exp\left(-\left(\frac{z}{z_0}\right)^\beta\right)\mathrm{d}z \text{ with } \frac{1}{n_0} = \frac{z_0}{\beta}\Gamma\left(\frac{3}{\beta}\right), \quad (12)$$

and is the approximate forecasted distribution of the *Euclid* mission (Amara & Réfrégier 2007). z_0 has been chosen to be $\simeq 0.64$ such that the median of the redshift distribution is 0.9. With these definitions, one can carry out a Limber projection (Limber 1954) of the weak lensing convergence for obtaining the angular convergence spectrum $C_\kappa(\ell)$,

$$C_\kappa(\ell) = \int_0^{\chi_H}\frac{\mathrm{d}\chi}{\chi^2}\,W_\kappa^2(\chi)P(k = \ell/\chi), \quad (13)$$

which describes the fluctuation statistics of the convergence field.

3 TOMOGRAPHY WITH ORTHOGONAL POLYNOMIALS

3.1 Motivation for tomography

Weak cosmic shear provides a measurement of the weighted, line of sight integrated tidal shears, although it is more convenient to work in terms of the weak lensing convergence and the cosmic density field, which have statistically equivalent properties. Weak lensing therefore provides an integrated measurement of the evolution of the cosmic density field weighted with the lensing efficiency function. Being a line of sight averaged quantity, the weak lensing convergence is statistically not as constraining as the full three-dimensional density field, which is caused by the mixing of spatial scales in the Limber projection. Additionally, parameters which enter the model in a non-linear way can cause different effects on the weak lensing signal at different redshifts. This sensitivity would be averaged out in a long-baseline line of sight integration and the information would be lost.

The solution to this problem is tomographic methods: splitting up the lensing signal from different distances allows a larger signal strength and a higher sensitivity with respect to cosmological parameters because the line of sight averaging effect is reduced. This comes at the cost of a more complicated covariance between the spectra measured, and a higher shape noise for each of the spectra, because the effective number of galaxies is reduced. There are different methods for exploiting evolution of the cosmic density field and the lensing sensitivity along the line of sight. Since the inception of tomography for investigating weak lensing convergence spectra (Hu 1999, 2002a) and bispectra (Takada & Jain 2004), there have been many developments leading ultimately to cross-correlation cosmography (Bernstein & Jain 2004), where a lensing template is derived from data and used to predict the weak shear signal on background sources, and to three-dimensional weak shear methods, which are an unbinned, direct mapping of the cosmological density field (Heavens 2003; Castro et al. 2005; Kitching et al. 2011).

Common to these methods is strong covariances between spectra, which we aim to avoid by employing a set of specifically designed polynomials, which perform a weighting of the observed ellipticities in their distance, in a way that convergence cross-spectra computed with two different polynomials vanishes. This ensures that every polynomial projects out information about the deflection field which is statistically independent, and generates a covariance matrix of a particular simple shape. In a sense, TaRDiS is using a non-local binning of the ellipticities motivated by the anticipated weak lensing signal, which corresponds to the non-local nature of weak lensing.

3.2 Construction of orthogonal sets of polynomials

We introduce a weighting of the distance distribution of the galaxies $n(\chi) = n(z)\,dz/d\chi = n(z)H(z)$ with a function $p_i(\chi)$, such that the lensing efficiency function reads

$$W_i(\chi) = \frac{3\Omega_{\mathrm{m}}}{2\chi_H^2}\frac{1}{a}G_i(\chi)\chi, \tag{14}$$

with

$$G_i(\chi) = \int_\chi^{\chi_H} d\chi'\, n(\chi')\, p_i(\chi')\, \frac{\chi'-\chi}{\chi'}. \tag{15}$$

A line-of-sight weighting of the weak lensing convergence with a function $p_i(\chi)$ yields the weighted convergence field κ_i,

$$\kappa_i = \int_0^{\chi_H} d\chi\, W_i(\chi)\delta(\chi), \tag{16}$$

from which one obtains for the variance between two Fourier modes $\kappa_i(\ell)$,

$$\left\langle \kappa_i(\ell)\kappa_j^*(\ell')\right\rangle = (2\pi)^2\delta_{\mathrm{D}}(\ell-\ell')S_{ij}(\ell), \tag{17}$$

with the weighted convergence spectrum $S_{ij}(\ell)$ for homogeneous and isotropic fluctuations of κ_i,

$$S_{ij}(\ell) = \int_0^{\chi_H} \frac{d\chi}{\chi^2}\, W_i(\chi)W_j(\chi)\, P(k = \ell/\chi, \chi). \tag{18}$$

As our statistical analysis will be dealing only with homogenous random fields, the CDM spectrum should be the one describing homogenous linear growth, $P(k, \chi) = D_+^2(\chi)P(k)$. In a few plots, however, we present the results for non-linear spectra $P(k, \chi)$ for which we employ the description by Smith et al. (2003). Additionally, we would like to point out that line-of-sight weightings with the polynomials $p_i(\chi)$ do not introduce correlations between different multipole orders in the convergence field, as they do not affect statistical homogeneity.

This expression provides the definition of a scalar product between the weighting functions $p_i(\chi)$ and $p_j(\chi)$ contained in $W_i(\chi)$ and $W_j(\chi)$, respectively,

$$\langle p_i, p_j\rangle \equiv S_{ij}(\ell), \tag{19}$$

which exhibits the necessary properties of being positive definite ($\langle p_i, p_i\rangle \geq 0$ and $\langle p_i, p_i\rangle = 0 \leftrightarrow p_i \equiv 0$), symmetric ($\langle p_i, p_j\rangle = \langle p_j, p_i\rangle$) and linear in both arguments. Starting point for the construction of orthogonal polynomials which would diagonalize $S_{ij}(\ell)$, $S_{ij}(\ell) \propto \delta_{ij}$, is the family monomials

$$p_i'(\chi) = \left(\frac{\chi}{\chi_{\mathrm{node}}}\right)^i, \tag{20}$$

where χ_{node} can be chosen for placing the node of the first polynomial in a sensible way, in our case it is set to the median value of the galaxy redshift distribution, converted into comoving distance. The monomials $p_i'(\chi)$ are subjected to a Gram–Schmidt orthogonalization procedure, with the initial condition

$$p_0(\chi) = p_0'(\chi) \equiv 1 \tag{21}$$

and, iteratively,

$$p_i(\chi) = p_i'(\chi) - \sum_{j=0}^{i-1} \frac{\langle p_i', p_j\rangle}{\langle p_j, p_j\rangle} p_j(\chi). \tag{22}$$

It should be emphasized that the orthogonalization procedure needs to be repeated for every multipole ℓ, and that we have omitted an additional index ℓ of the polynomials $p_i(\chi)$ for clarity. For illustration the polynomials are normalized using the norm induced by the scalar product defined in equation (19),

$$p_i(\chi) \leftarrow \frac{p_i(\chi)}{\sqrt{\langle p_i, p_i\rangle}}, \tag{23}$$

which appears in the denominator of equation (22) in a natural way. Clearly, the scalar product $S_{ij}(\ell)$ is equal to the convergence spectrum $C_\kappa(\ell)$ for $i = j = 0$, in which case $p_0 \equiv 1$. This means that the non-tomography case is recovered for $i = 0$ and that the tomographic modes are obtained for $i \geq 1$, which will by construction all constitute statistically independent measurements.

3.3 Properties of orthogonal polynomials

Fig. 1 shows the polynomials $p_i(\chi)$ at a fixed multipole order of $\ell = 1000$. They exhibit a sequence of oscillations roughly at the
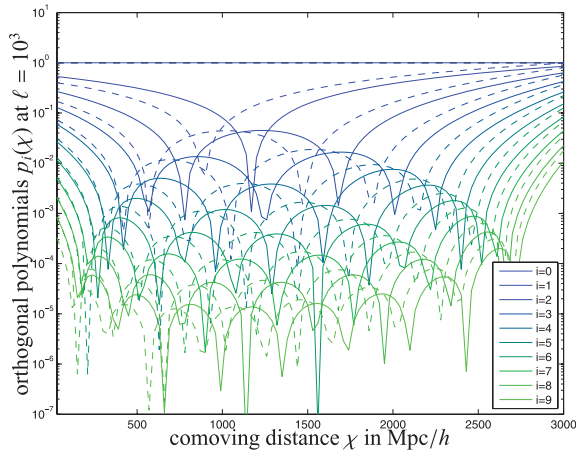
Figure 1. Orthogonal polynomials $p_i(\chi)$, $i = 0, \ldots, 9$, as a function of comoving distance χ constructed with the Gram–Schmidt algorithm for the weak lensing spectrum at $\ell = 10^3$, with the lowest order polynomials on top, for both a linear (solid line) and a non-linear (dashed line) CDM spectrum $P(k)$.

positions where the previous polynomial assumes their maximal values. When computing the polynomials for the non-linear CDM spectrum instead for the linear one, the sequence of oscillations is shifted to smaller comoving distances. The reason for this shift is the larger amplitude of the non-linear spectrum $P(k)$ for small $k = \ell/\chi$, which causes a larger contribution of the weak lensing spectrum to be generated at high χ. We emphasize that the polynomial for $i = 0$, which corresponds to a constant weighting along the line of sight and hence to the non-tomographic case, yields a constant $p_0(\chi) = 1$.

The variation of the polynomials $p_i(\chi)$ with distance χ and multipole order ℓ is depicted in Fig. 2, in this case for the polynomial $i = 9$. Again, small variations with multipole order ℓ are present, and the oscillations when varying χ are clearly seen. Typically, differences between polynomials $p_i(\chi)$ tend to be larger at low multipoles in comparison to high multipole orders. These differences are larger than those introduced by changes in the fiducial cosmological model of the order of the target precision needed for parameter estimation which leads us to conclude that a separate orthogonalization of each ℓ mode is necessary.
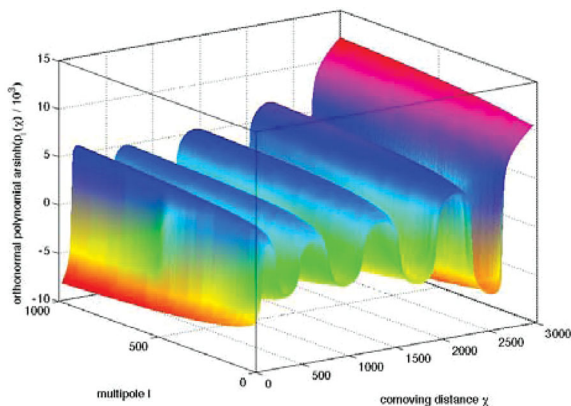

Figure 2. Orthonormal polynomials $p_i(\chi)$ as a function of multipole order ℓ and comoving distance χ. The order of the polynomial has been fixed to $i = 9$ and was constructed for a non-linear CDM spectrum. One can see the slow variation of the $p_i(\chi)$ polynomials with multipole order ℓ.
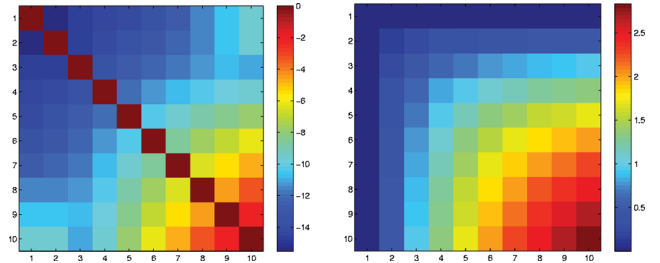

Figure 3. Orthonormality relation for the polynomials $p_i(\chi)$, at $\ell = 10^3$ in logarithmic representation, for the signal covariance S_{ij} (left-hand panel) and the noise covariance N_{ij} (right-hand panel), for the *Euclid* survey characteristics, in units of the shape noise $\sigma_\epsilon^2/\bar{n}$.

The orthonormality relation $\langle p_i, p_j \rangle$ of the polynomials $p_i(\chi)$ for the lensing signal as well as for the galaxy shape noise is given in Fig. 3. The polynomials are constructed to be orthogonal by the Gram–Schmidt procedure, but numerical noise is collected in the iterative process, such that the orthogonality relation is better fulfilled at small i compared to larger i. Deviations from $\langle p_i, p_j \rangle = 0$ for $i \neq j$ are of the order of $\sim 10^{-15}$ for low-order polynomials, but increase to values of $\sim 10^{-4}$ at high order. This deterioration in orthogonality is a known drawback of the Gram–Schmidt procedure, in particular when dealing with sets of functions instead sets of vectors, which means that there is larger numerical noise due to a twofold numerical integration in the evaluation of the scalar products. The failure of the Gram–Schmidt algorithm to provide properly orthogonalized basis polynomials for higher orders exceeding $i \geq 10$ is the reason why we focus on the low orders, in addition they are the ones that will be carrying most of the statistical information.

One can already notice the main difference between the different approaches in tomography: whereas the noise covariance would be diagonal in classic tomography with a very complicated structure of the signal covariance, in our case the shapes of the signal and noise covariance matrix are interchanged.

Fig. 4 gives an impression of the lensing efficiency function $W_i(\chi)$ modified by the polynomials $p_i(\chi)$ on an angular scale of $\ell = 1000$, in comparison to that of weak shear without tomography, $W_0(\chi) \equiv W_\kappa(\chi)$ for $i = 0$. It is quite interesting to see how the seemingly messy functions $W_i(\chi)$ disentangle and approach zero at large distances.
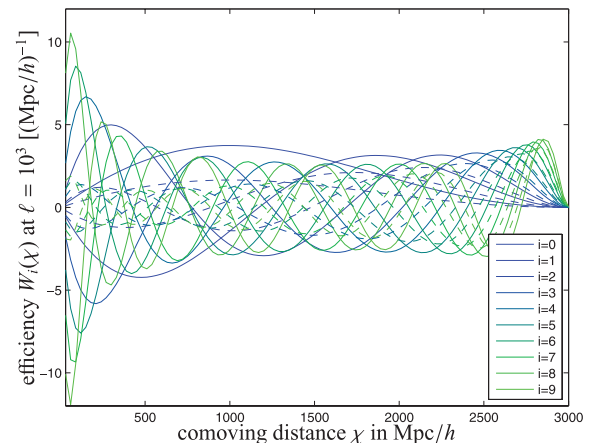

Figure 4. Lensing efficiency functions $W_i(\chi)$, $i = 0, \ldots, 9$, as a function of comoving distance χ, for both linear (solid line) and non-linear (dashed line) CDM spectra. The lensing efficiency functions have been constructed for $\ell = 10^3$.
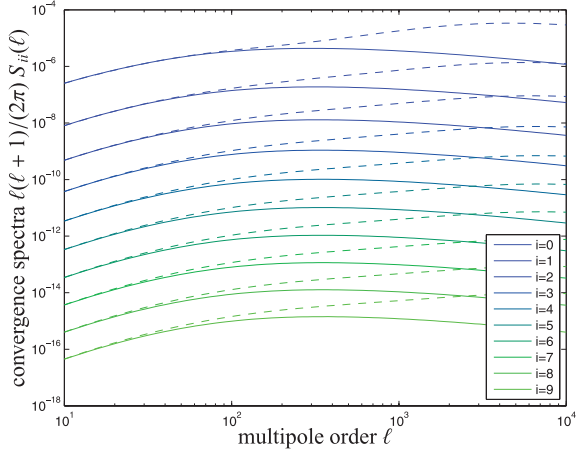
Figure 5. Weak lensing spectra $S_{ii}(\ell)$, $i = 0, \ldots, 9$, weighted with orthogonal polynomials $p_i(\chi)$, as a function of multipole order ℓ, for both a linear (solid line) and a non-linear (dashed line) CDM spectrum $P(k)$. The spectra decrease in amplitude with increasing polynome order i for unnormalized polynomials.

Finally, polynomial-weighted weak lensing spectra $S_{ii}(\ell) = \langle p_i, p_j \rangle$ are shown in Fig. 5. The spectra drop in amplitude, which is mostly an effect of the absence of normalization, and there are in fact differences in shape, when higher order polynomials are used (compare Fig. A1 in the appendix, where all spectra are scaled such that they assume the same value at a certain multipole). By construction, these spectra provide statistically independent information of the cosmic large-scale structure. In the next sections, we will investigate statistical bounds and systematical errors on cosmological parameters, when the information from different spectra is combined.

4 STATISTICAL ERRORS

In this section we show how we construct covariance matrices for the polynomial-weighted spectra, compute the Fisher matrix and derive statistical errors on cosmological parameters and investigate the signal strength of the weak shear signal, all as a function of the number of polynomials used.

4.1 Variances of weighted ellipticities

For deriving the expressions for the signal covariance and the noise covariance needed in forecasting statistical and systematical errors, we derive expressions for the mean and the variance for a weighted set of ellipticities. This derivation is done for a discrete set of weighting coefficients w_m and then generalized to the continuous case, where the weighting is done with a polynomial $p_i(\chi)$. The distribution $p(\epsilon)\,d\epsilon$ of ellipticities ϵ is assumed to be Gaussian, with a zero mean, variance σ_ϵ and the ellipticities are taken to be intrinsically uncorrelated (i.e. intrinsic alignment effects are discarded, see Schäfer 2009, for a review).

From a measurement of a set of ellipticities ϵ_m drawn from the parent distribution $p(\epsilon)\,d\epsilon$ one can estimate the shear by computing the weighted mean $\bar{\epsilon}$, and the expectation value of the weighted mean $\langle \bar{\epsilon} \rangle$ if the drawing of ellipticities is repeated,

$$\bar{\epsilon} = \frac{\sum_m w_m \epsilon_m}{\sum_m w_m} \rightarrow \langle \bar{\epsilon} \rangle = \frac{\sum_m w_m \langle \epsilon_m \rangle}{\sum_m w_m} = 0, \tag{24}$$

which vanishes if the mean ellipticity vanishes, $\langle \epsilon_m \rangle = 0$. For the variance $\langle \bar{\epsilon}^2 \rangle$ one obtains under the assumption of intrinsically uncorrelated ellipticities, $\langle \epsilon_m \epsilon_n \rangle = \sigma_\epsilon^2 \delta_{mn}$,

$$\langle \bar{\epsilon}^2 \rangle = \frac{1}{\sum_m w_m \sum_n w_n} \sum_{mn} w_m w_n \langle \epsilon_m \epsilon_n \rangle = \frac{\sigma_\epsilon^2}{\left(\sum_m w_m\right)^2} \sum_m w_m^2, \tag{25}$$

which reduces to the classic Poissonian result if w_m is either 0 or 1,

$$\langle \bar{\epsilon}_{ww}^2 \rangle = \frac{\sigma_\epsilon^2}{N} \quad \text{with} \quad N = \sum_m w_m, \tag{26}$$

because $w_m^2 = w_m$, and N is defined as the effective number of ellipticities in the sample. The cross-variance for two different sets of weights w_m and v_n is given by

$$\langle \bar{\epsilon}^2 \rangle = \frac{\sigma_\epsilon^2}{\sum_m w_m \sum_n v_n} \sum_m w_m v_m. \tag{27}$$

In the continuum limit we make the transition

$$\sum_m \cdots \rightarrow \bar{n} \int d\chi \, n(\chi) \cdots, \tag{28}$$

with the unit normalized galaxy distance distribution $n(\chi)\,d\chi$. The discrete weights w_m and v_m will be replaced by the set of polynomials $p_i(\chi)$ and $p_j(\chi)$. For conserving the normalization of the weighted galaxy distance distribution $n(\chi)\,d\chi$, we normalize the polynomials

$$p_i(\chi) \leftarrow \frac{p_i(\chi)}{\int d\chi \, n(\chi) p_i(\chi)}, \tag{29}$$

such that the weak shear spectrum $S_{ij}(\ell)$ becomes

$$S_{ij} = \langle p_i, p_j \rangle = \int_0^{\chi_H} \frac{d\chi}{\chi^2} \, W_i(\chi) W_j(\chi) \, P(k = \ell/\chi), \tag{30}$$

which is diagonal by construction, and the noise covariance,

$$N_{ij} = \frac{\sigma_\epsilon^2}{\bar{n}} \int d\chi \, n(\chi) p_i(\chi) p_j(\chi), \tag{31}$$

with the shape noise σ_ϵ and the mean density of galaxies $\bar{n}$ per steradian, for which we substitute the numbers $\sigma_\epsilon = 0.3$ and $\bar{n} = 40 \, \text{arcmin}^{-2}$ projected for *Euclid*. It can already be seen from the expression for N_{ij} that the weighting of data with high-order polynomials $p_i(\chi)$ will be noisy: $n(\chi)$ is a slowly varying function and the integrals $\int d\chi \, n(\chi) p_i(\chi)$ in the denominator will assume small values if the polynomial is rapidly oscillating. This will ultimately limit the order of the usable polynomials. Again, for $i = j = 0$, the standard Poissonian expression $N_{00} = \sigma_\epsilon^2/\bar{n}$ is recovered due to the normalization of $n(z)$, as well as the weak shear spectrum $S_{00}(\ell) = C_\kappa(\ell)$.

4.2 Fisher analysis

The likelihood function for observing Gaussian-distributed uncorrelated modes $\kappa_i(\ell)$ of the $p_i(\chi)$-weighted weak lensing convergence for a given parameter set x_μ is defined as (see Tegmark, Taylor & Heavens 1997; Carron, Amara & Lilly 2011)

$$\mathcal{L}(\kappa_i(\ell)|x_\mu) = \frac{1}{\sqrt{(2\pi)^N \det(\mathbf{C})}} \exp\left(-\frac{1}{2}\kappa_i(\ell) C_{ij}^{-1}(\ell, \ell')\kappa_j^*(\ell')\right), \tag{32}$$

with the covariance $C_{ij}(\ell, \ell') \equiv \langle \kappa_i(\ell)\kappa_j^*(\ell') \rangle$ which is diagonal in ℓ for homogeneous random fields. We choose to work with the weak lensing convergence κ as it has the same statistical properties as the E-mode spectrum of the weak lensing shear, and work in the

approximation that the difference between shear and reduced shear is small.

The χ^2 functional, $\mathcal{L} \propto \exp(-\chi^2/2)$, can be obtained from the logarithmic likelihood and reads

$$\chi^2 = \sum_\ell \mathrm{tr} \left[\ln \mathbf{C} + \mathbf{C}^{-1} \mathbf{D} \right], \tag{33}$$

with the definition of the data matrix $D_{ij} = \kappa_i(\boldsymbol{\ell})\kappa_j(\boldsymbol{\ell})$, using the relation $\ln \det(\mathbf{C}) = \mathrm{tr} \ln(\mathbf{C})$ and discarding irrelevant multiplicative pre-factors. The second derivatives of the χ^2 functional with respect to cosmological parameters x_μ evaluated at the point of maximum likelihood yield the Fisher matrix

$$F_{\mu\nu} = -\left\langle \frac{\partial^2}{\partial x_\mu \partial x_\nu} \frac{\chi^2}{2} \right\rangle = \sum_\ell \frac{2\ell+1}{2} \mathrm{tr} \left(\frac{\partial}{\partial x_\mu} \ln \mathbf{C} \frac{\partial}{\partial x_\nu} \ln \mathbf{C} \right), \tag{34}$$

with multiplicity $2\ell + 1$ because on each angular scale ℓ there are $2\ell + 1$ statistically independent m modes. The covariance $C_{ij} = S_{ij} + N_{ij}$ can be split up into the signal covariance S_{ij},

$$S_{ij}(\ell) = \begin{pmatrix} S_{00}(\ell) = C_\kappa(\ell) & & 0 \\ & \ddots & \\ 0 & & S_{qq}(\ell) \end{pmatrix}, \tag{35}$$

and the noise covariance N_{ij},

$$N_{ij}(\ell) = \begin{pmatrix} N_{00}(\ell) = \sigma_\epsilon^2/\bar{n} & \cdots & N_{q0}(\ell) \\ \vdots & \ddots & \vdots \\ N_{0q}(\ell) & \cdots & N_{qq}(\ell) \end{pmatrix}. \tag{36}$$

We will work in the limit $\partial S_{ij}/\partial x_\mu \gg \partial N_{ij}/\partial x_\mu$ which is well justified in our case. After these steps, the signal covariance S_{ij} assumes a diagonal shape in ℓ because of statistical homogeneity of the $\kappa_i(\ell)$ modes does not depend on the direction of $\boldsymbol{\ell}$ because of statistical isotropy and diagonal in the polynomial index, because of the construction of the polynomials to yield a diagonal signal covariance, which does not interfere with property of being statistically homogeneous. Non-linear structure formation, however, will render the modes of the convergence field correlated. In contrast, the noise covariance N_{ij} cannot brought to diagonal shape in i at the same time, and therefore N_{ij} will be a symmetric matrix with no particular further properties.

Fig. 6 gives an example of how the combination of multiple line of sight weighted measurements helps to avoid weaknesses in the sensitivity towards cosmological parameters. We plot the sensitivity

$$\sqrt{\mathrm{tr} \left(\frac{\partial \ln \mathbf{C}}{\partial x_\mu} \right)^2} = \sqrt{\frac{2}{2\ell+1} \frac{\mathrm{d}F_{\mu\mu}}{\mathrm{d}\ell}}, \tag{37}$$

i.e. the ratio between the derivative of the spectrum with respect to a cosmological parameter and the covariance of the measurement, which corresponds to the contributions to the diagonal elements of the Fisher matrix per ℓ mode. The sensitivities of the measurement with respect to the cosmological parameters Ω_m and w are shown, which exhibit singularities at certain multipoles for a classical non-tomographic measurement. This happens when a parameter affects a certain ℓ range with a different sign than others and the spectrum pivots around this value when varying a parameter. Clearly, angular scales in the vicinity of that pivot scale do not add much sensitivity to the Fisher matrix. The inclusion of a second polynomial, however, avoids this: for $q \geq 1$ on, singularities are lifted and the derivatives assume larger values with increasing numbers
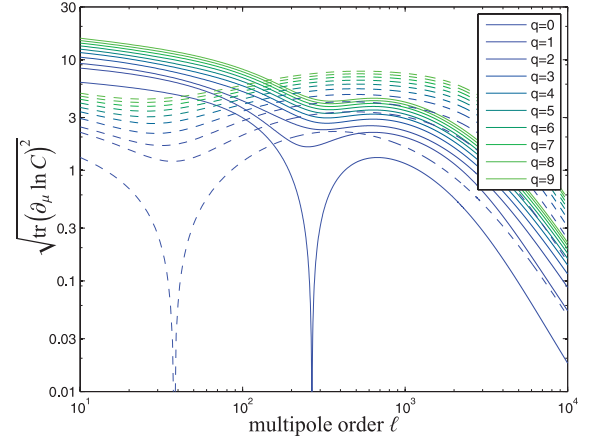

Figure 6. Derivatives $\sqrt{\mathrm{tr}(\partial_{\Omega_m} \ln \mathbf{C})^2}$ (solid lines) and $\sqrt{\mathrm{tr}(\partial_w \ln \mathbf{C})^2}$ (dashed lines) as a function of multipole order ℓ and cumulative polynomial order q. The derivatives have been weighted with the *Euclid* covariance.

of polynomials, although this effect saturates for very large numbers of polynomials. At large multipoles, the influence of the shape noise can be observed, which causes the derivatives to drop rapidly, and do not add significant sensitivity to the Fisher matrix on scales larger than $\ell \simeq 3000$.

4.3 Statistical errors

From the Fisher matrix $F_{\mu\nu}$ one can obtain the Cramér–Rao errors,

$$\sigma_\mu^2 = (\mathbf{F}^{-1})_{\mu\mu}, \tag{38}$$

and the two-dimensional marginalized logarithmic likelihood χ_m^2 around the fiducial model x_μ^*,

$$\chi_m^2 = \begin{pmatrix} x_\mu - x_\mu^* \\ x_\nu - x_\nu^* \end{pmatrix}^t \begin{pmatrix} (F^{-1})_{\mu\mu} & (F^{-1})_{\mu\nu} \\ (F^{-1})_{\nu\mu} & (F^{-1})_{\nu\nu} \end{pmatrix}^{-1} \begin{pmatrix} x_\mu - x_\mu^* \\ x_\nu - x_\nu^* \end{pmatrix}. \tag{39}$$

Fig. 7 summarizes statisticalerrors on cosmological parameters resulting from the Fisher matrix analysis, cumulative in q and for
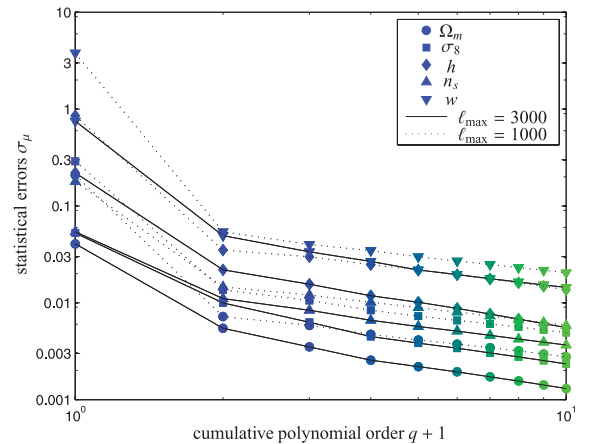

Figure 7. Statistical errors on the estimates of the cosmological parameters Ω_m (circles), σ_8 (squares), h (lozenges), n_s (triangles, pointing up) and w (triangles, pointing down) resulting as Cramér–Rao errors from computing the Fisher matrix for the weak lensing spectrum $S_{ii}(\ell)$, as a function of cumulative polynomial order q, for *Euclid* survey characteristics. The maximum multipole considers is $\ell_{max} = 1000$ (dotted lines) and $\ell_{max} = 3000$ (solid lines).
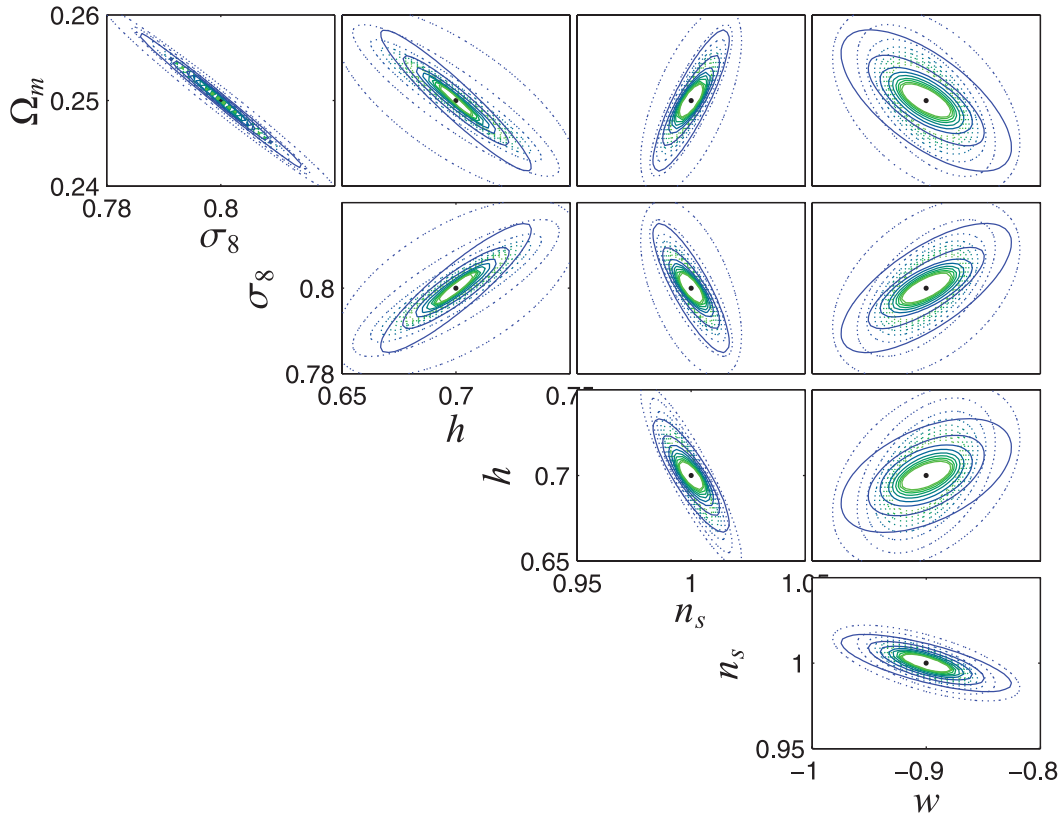
Figure 8. Constraints on the cosmological parameters Ω_m, σ_8, h, n_s and w from *Euclid* using tomography with orthogonal polynomials. The ellipses mark 1σ confidence regions and decrease in size with increasing cumulative polynomial order ($q = 0$ in blue to $q = 9$ in green), for $\ell_{max} = 1000$ (dotted lines) and $\ell_{max} = 3000$ (solid lines). The case $q = 0$ corresponds to an unweighted, non-tomographic spectrum of the weak lensing convergence κ.

$\ell = 1000$ as well as for $\ell = 3000$. As expected, statistical errors drop with larger number of polynomials and are smaller if more multipoles are considered. A very fascinating feature of the plot is the approximate scaling of the error with the inverse root of the number of polynomials, $\sigma \propto 1/\sqrt{q}$, which one expects from Poissonian arguments because each spectrum $S_{ii}(\ell)$ adds statistically independent information. Because of numerical noise in the Gram–Schmidt procedure it is very difficult to extend the analysis beyond $q \geq 10$ as the polynomials are not properly orthogonal at high orders.

Two-dimensional marginalized likelihoods for all parameter pairs are shown in Fig. 8, for $\ell = 1000$ and 3000 as the maximum multipole considered. In the confidence contours, up to 10 polynomials were combined. Clearly, the uncertainty in cosmological parameters decreases with larger numbers of polynomials used, as well as for an increased multipole range. Additionally, the parameter degeneracies change a little when more polynomials are used, which is caused by differing sensitivities of the lensing signal with distance. A three-dimensional view of the marginalized likelihood of the parameters Ω_m, σ_8 and w is given in Fig. 9. It illustrates nicely the nested 1σ ellipsoids which become smaller for larger number of polynomials combined in the measurement.

At this point we emphasize that our estimates for statistical errors relies on statistically independent modes, which is only applicable as long as the density field is in the linear stage of structure formation. Correlations between modes generates additional contribution to the covariance which impacts on the magnitude of derived statistical errors as well as on the signal strength, weaking both quantities (Takada & Jain 2009).
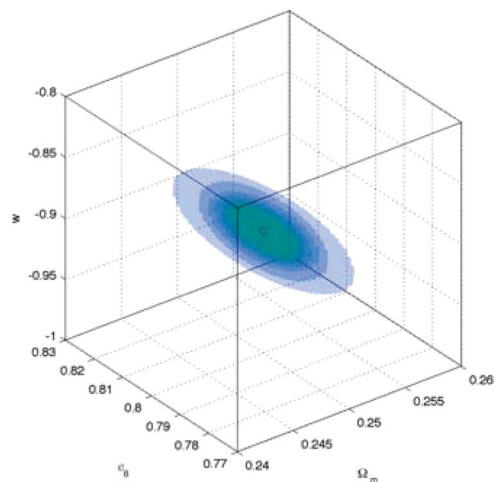

Figure 9. 1σ ellipsoids in the space spanned by (Ω_m, σ_8, w), cumulative in polynomial order q, from $q = 2$ (largest ellipsoid) up to $q = 9$ (smallest ellipsoid) with the maximum multipole order set to $\ell = 3000$. Observational characteristics correspond to those of the *Euclid* mission.

Comparing the performance of the TaRDiS polynomials to other tomographic methods shows that they operate on very similar levels of performance, perhaps with a small advantage for the cosmological parameters Ω_m and w. This is due to the mechanism that the values in the Fisher matrix are maximized if the covariance becomes diagonal due to a match between the true cosmology and the
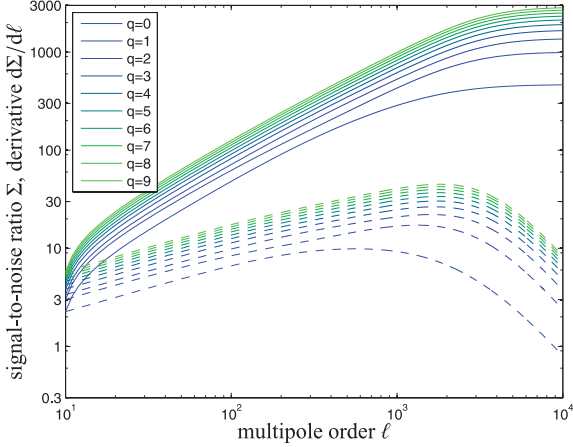
Figure 10. Signal-to-noise ratio $\Sigma(\ell)$ (solid lines) and the contribution $d\Sigma/d\ell$ by each multipole (dashed lines) as a function of inverse angular scale ℓ and cumulative polynomial order q. The shape noise corresponds to that of the projected *Euclid* performance.

assumed cosmology used for constructing the polynomials. This should be taken with a grain of salt, however, because part of the statistical error would be transported to the systematical error budget. The impact of starting off with a wrong cosmological model for construction of the TaRDiS polynomials on the estimation of parameters will be the topic of the next chapter.

4.4 Signal-to-noise ratio

Analogous to the definition of the Fisher matrix we construct the cumulative signal-to-noise ratio Σ,

$$\Sigma^2 = \sum_\ell \frac{2\ell+1}{2} \mathrm{tr}\left(\mathbf{C}^{-1}\mathbf{S}\mathbf{C}^{-1}\mathbf{S}\right) = \sum_\ell \frac{2\ell+1}{2} \mathrm{tr}\left(\mathbf{C}^{-1}\mathbf{S}\right)^2, \quad (40)$$

from the covariance matrices with the multiplicity $2\ell+1$. The cumulative signal-to-noise ratio Σ and the differential contribution $d\Sigma/d\ell$ of each multipole are summarized in Fig. 10. Clearly, increasing q or ℓ increases the signal up to multipole orders of a few thousand. The growth of $d\Sigma(\ell)/d\ell \propto \sqrt{2\ell+1}$ is driven by the reduced cosmic variance until the shape noise limits the measurability of the spectra. Consequently, the integrated signal-to-noise ratio settles off at a few hundred, and adding statistically independent information by using new polynomials increases the signal strength by almost an order of magnitude and reaches values comparable to the primary CMB temperature anisotropy spectrum (Hu 2002a). These numbers correspond well to those derived by Takada & Jain (2009) if one works in the approximation of a Gaussian covariance – non-Gaussian contributions can significantly lower the signal strength by introducing a proportionality to the trispectrum of the convergence field. This can be expected from equation (40), as the signal-to-noise ratio is invariant under orthogonal transformations diagonalizing either S_{ij} or N_{ij}.

5 SYSTEMATICAL ERRORS

Naturally, the set of polynomials used for analysing the data needs to be constructed for specific cosmology, so the question arises if an imprecise prior knowledge of the cosmological model has an impact on the parameter estimates from the weighted weak lensing spectra. Any incompleteness or imperfection in the model used for interpreting the data is going to shift the estimated parameter values

away from their true values and introduces parameter estimation biases. Specifically, we consider three cases.

First, a time-varying equation of state ($w = -0.8 + 0.2(1 - a)$) when in reality the equation of state of dark energy is constant ($w = -0.9$), i.e. a systematic which is not a degree of freedom of the model, and secondly wrongly assumed Ω_m and σ_8 values (0.3 instead of 0.25 and 0.85 instead of 0.8, respectively) as a strong systematic. In addition, we compute biases in the estimation of cosmological parameters if the redshift distribution of galaxies substituted in the polynomial construction is not the true one.

5.1 Parameter estimation bias

For the Gaussian likelihood function $\mathcal{L} \propto \exp(-\chi^2/2)$ for a parabolic χ^2 functional one can identify $\chi^2 \equiv \sum_\ell \mathrm{tr}\left[\ln\mathbf{C} + \mathbf{C}^{-1}\mathbf{D}\right]$ with the covariance C_{ij} and the data matrix D_{ij}. Now, the fit of the true model $\mathbf{C}_t$ to the data would give rise to the correct χ_t^2 functional,

$$\chi_t^2 = \sum_\ell \mathrm{tr}\left[\ln\mathbf{C}_t + \mathbf{C}_t^{-1}\mathbf{D}\right], \quad (41)$$

whereas the assumption of a wrong model yields

$$\chi_f^2 = \sum_\ell \mathrm{tr}\left[\ln\mathbf{C}_f + \mathbf{C}_f^{-1}\mathbf{D}\right], \quad (42)$$

which in general will assume its global minimum at parameter values different than χ_t^2. The distance $\boldsymbol{\delta}$ between the best-fitting values $\boldsymbol{x}_t$ of the true model and $\boldsymbol{x}_f$ of the false model will then be the parameter estimation bias. This parameter estimation bias can be quantified with a second-order Taylor expansion of the χ_f^2 functional for the wrong model around the best-fitting point $\boldsymbol{x}_t$ of the true model (see Cabré et al. 2007):

$$\chi_f^2(\boldsymbol{x}_f) = \chi_f^2(\boldsymbol{x}_t) + \sum_\mu \frac{\partial}{\partial x_\mu}\chi_f^2(\boldsymbol{x}_t)\delta_\mu + \frac{1}{2}\sum_{\mu,\nu}\frac{\partial^2}{\partial x_\mu \partial x_\nu}\chi_f^2(\boldsymbol{x}_t)\delta_\mu\delta_\nu, \quad (43)$$

where the parameter estimation bias vector $\boldsymbol{\delta} \equiv \boldsymbol{x}_f - \boldsymbol{x}_t$. The best-fitting position $\boldsymbol{x}_f$ of χ_f^2 can be recovered by extremization of the ensemble averaged $\langle\chi_f^2\rangle$, yielding

$$\underbrace{\left\langle\frac{\partial}{\partial x_\mu}\chi_f^2\right\rangle_{\boldsymbol{x}_t}}_{\equiv a_\mu} = \sum_\nu \underbrace{-\left\langle\frac{\partial^2}{\partial x_\mu \partial x_\nu}\chi_f^2\right\rangle_{\boldsymbol{x}_t}}_{\equiv G_{\mu\nu}}\delta_\nu, \quad (44)$$

which is a linear system of equations of the form

$$\sum_\nu G_{\mu\nu}\delta_\nu = a_\mu \rightarrow \delta_\mu = \sum_\nu (G^{-1})_{\mu\nu}a_\nu, \quad (45)$$

where the two quantities $G_{\mu\nu}$ and a_μ follow from the derivatives of the averaged χ_f^2 functional, evaluated at $\boldsymbol{x}_t$, with $\langle\mathbf{D}\rangle = \mathbf{C}_t$ and the multiplicity $2\ell+1$ added for each ℓ mode:

$$a_\mu = \sum_\ell \frac{2\ell+1}{2}\mathrm{tr}\left[\frac{\partial}{\partial x_\mu}\ln\mathbf{C}_f\left(\mathrm{id} - \mathbf{C}_f^{-1}\mathbf{C}_t\right)\right]. \quad (46)$$

This vector reduces to $a_\mu = 0$ if $\mathbf{C}_t = \mathbf{C}_f$ (id being the identity matrix). Furthermore,

$$G_{\mu\nu} = \sum_\ell \frac{2\ell+1}{2}\mathrm{tr}\left[\mathbf{C}_f^{-1}\frac{\partial^2}{\partial x_\mu \partial x_\nu}\mathbf{C}_f\left(\mathbf{C}_f^{-1}\mathbf{C}_t - \mathrm{id}\right)\right]$$
$$- \sum_\ell \frac{2\ell+1}{2}\mathrm{tr}\left[\frac{\partial}{\partial x_\mu}\ln\mathbf{C}_f\frac{\partial}{\partial x_\nu}\ln\mathbf{C}_f\left(2\mathbf{C}_f^{-1}\mathbf{C}_t - \mathrm{id}\right)\right], \quad (47)$$
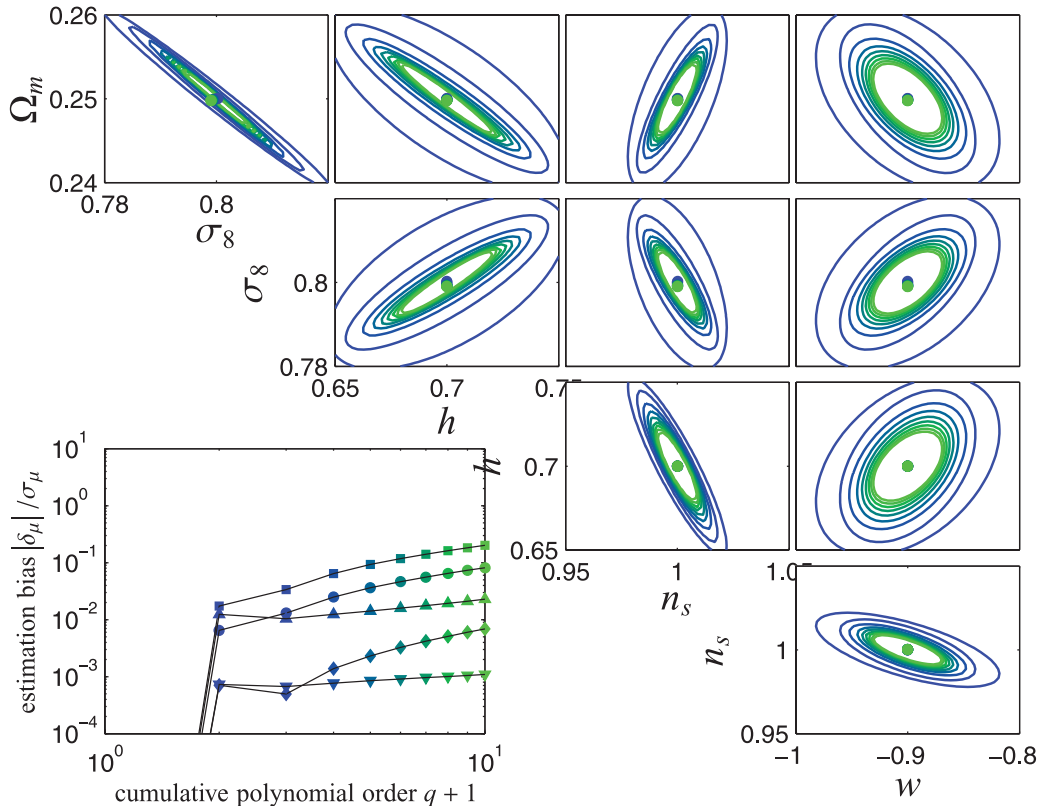
Figure 11. Parameter estimation biases (δ_μ, δ_ν) in the parameters Ω_m, σ_8, h, n_s and w, superimposed on the 1σ confidence regions, if the polynomials $p_i(\chi)$ have been constructed for wCDM with an evolving equation of state parametrized by $w_0 = -0.8$ and $w_a = -0.2$ instead of wCDM with a constant equation of state with $w = -0.9$. In the estimation biases, the dot colour is proportional to the cumulative order q of the polynomials, and is plotted again as a function of q for Ω_m (dots), σ_8 (squares), h (lozenges), n_s (triangles, pointing up) and w (triangles, pointing down). For all computations, the *Euclid* survey characteristics were used, and the data were accumulated up to $\ell_{max} = 1000$.

which simplifies to $G_{\mu\nu} = F_{\mu\nu}$ in the case of choosing the correct model, such that the parameter estimation bias vanishes. The same happens for $q = 0$, i.e. if only the polynomial $p_0(\chi) \equiv 1$ is used. In the derivation outlined above, the identities

$$\frac{\partial}{\partial x_\mu} \ln \mathbf{C} = \mathbf{C}^{-1} \frac{\partial}{\partial x_\mu} \mathbf{C} \quad \text{and} \quad \frac{\partial}{\partial x_\mu} \mathbf{C}^{-1} = -\mathbf{C}^{-1} \left(\frac{\partial}{\partial x_\mu} \mathbf{C} \right) \mathbf{C}^{-1} \tag{48}$$

were used. This formalism is a generalization of the case of diagonal covariance matrices (Cabré et al. 2007; Amara & Réfrégier 2008; Taburet et al. 2009; March et al. 2011), for which it has been shown to work well by comparison with results from Monte Carlo Markov chains (Taburet, Douspis & Aghanim 2010). We need to employ this more general formalism because the signal covariance $S_{ij}(\ell)$ ceases to be diagonal if the cosmology used for constructing the polynomials differs from the true cosmology. Other examples of non-diagonal covariances include three-dimensional cosmic shear (Heavens 2003; Kitching, Taylor & Heavens 2008). It should be emphasized that we are only investigating the impact of systematics or a wrongly chosen initial cosmology on the construction of polynomials and that systematics control plays a very important role in parameter estimation from weak lensing (among others, see King & Schneider 2002; Huterer et al. 2006; Bridle & King 2007; Semboloni et al. 2011), which we are not touching here.

5.2 Systematical errors

We constructed TaRDiS polynomials for three wrong assumptions: as the first example, we consider a rather small change in the dark

energy model, namely a time varying equation of state instead of a constant one. These two cosmologies have the same average dark energy equation of state, but the degree of freedom of a time varying w is contained in the true cosmology. For this case, Fig. 11 shows the estimation bias in the true dark energy model, when the model used for constructing the polynomials had been a time varying equation of state with the same average equation of state parameter. The figure illustrates that such a mistake has a minor impact on the estimation of parameters, as biases are smaller compared to the statistical precision by at least an order of magnitude. Most estimation bias can be found in the normalization σ_8.

Biases in the estimation of cosmological parameters if for the construction of the polynomials the wrong values for Ω_m and σ_8 have been used are summarized in Fig. 12. This case is a much stronger systematic compared to the previous case. There are strong biases in particular in Ω_m and σ_8, and to a lesser extend in n_s, whereas h and w are not strongly affected. Furthermore, the biases in Ω_m and σ_8 are in a direction almost orthogonal to the orientation of the degeneracy, indicating a particularly strong impact. These estimation biases, however, can be reduced by including a larger number of polynomials. In that way, a reduction of the bias to values similar to the statistical error is possible.

Finally, biases due to using a convolved redshift distribution in the polynomial construction whereas the signal is in reality generated by the unconvolved redshift distribution have been computed in Fig. 13. As a very simple model for the error in the measurement of the galaxy redshift distribution $n(z)\,\mathrm{d}z$ we used the convolution
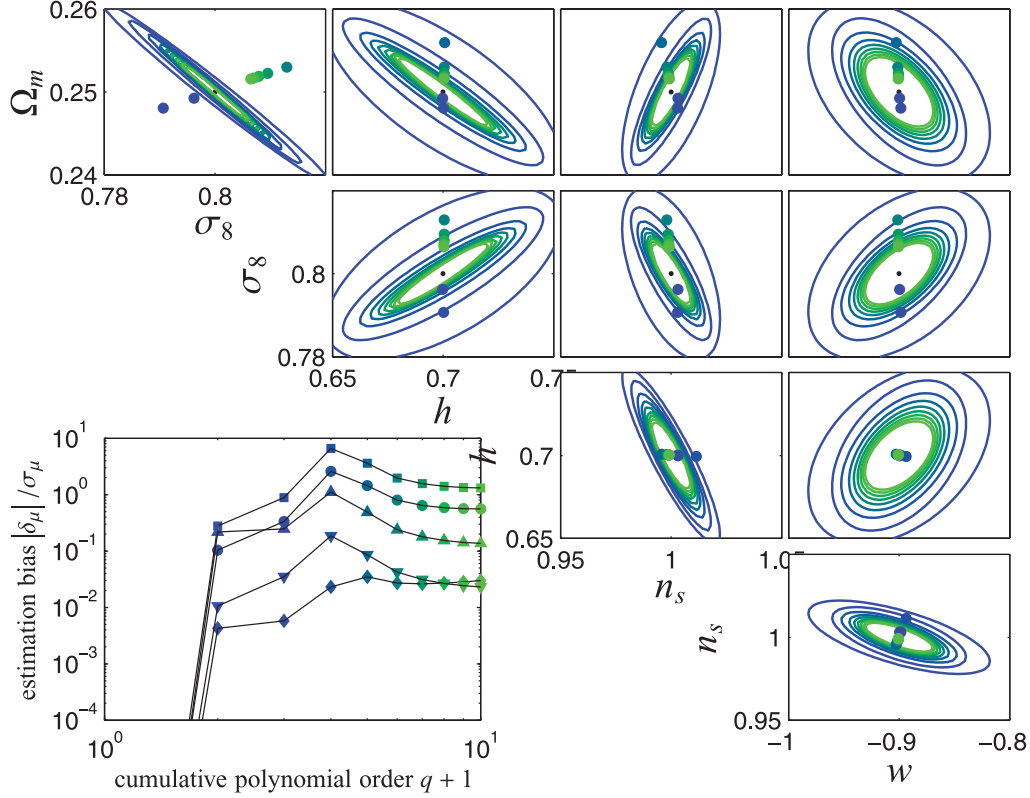
Figure 12. Parameter estimation biases (δ_μ, δ_ν) in the cosmological parameters Ω_m, σ_8, h, n_s and w, superimposed on the 1σ confidence regions, if in the construction of the polynomials Ω_m and σ_8 was set too high (0.275 and 0.85 instead of 0.25 and 0.8, respectively) relative to the fiducial cosmology. The colour of the dots indicates the cumulative polynomial order q for Ω_m (dots), σ_8 (squares), h (lozenges), n_s (triangles, pointing up) and w (triangles, pointing down). For the plot, *Euclid* survey characteristics were assumed, and the signal integrated up to $\ell_{max} = 1000$.

with a Gaussian (Ma, Hu & Huterer 2006),

$$r(z) = \frac{1}{\sqrt{2\pi\sigma_z^2}} \exp\left(-\frac{z^2}{2\sigma_z^2}\right) \quad \text{with} \quad \sigma_z = 0.05, \qquad (49)$$

which is of course too coarse to model errors in a proper weak lensing measurement, but will serve as an example. In contrast to the previous example, systematical errors in the parameters increase with larger numbers of polynomials used, and reach values of the order of the statistical error, in particular for Ω_m and σ_8, and to a lesser extend h. Quite similarly, the direction of the bias moves the best-fitting point quickly away from the true cosmology because it is at roughly right angles relative to the degeneracy direction.

Given the magnitude of systematical errors in comparison to their statistical accuracies, parameter estimation biases due to a wrongly chosen cosmology appear unlikely to affect measurements. In particular, if values estimated from unweighted tomography are used, the cosmological parameters are known well enough that TaRDiS polynomials can be constructed in a reliable way and consequent parameter estimation biases would always be subdominant in relation to the statistical errors. In addition, it is always possible to iterate between parameter estimation and polynomial construction for narrowing down estimation biases.

5.3 Cross-validation

A possible way of validating the correctness of the assumed cosmology for the construction of the orthogonal set of polynomials would be to estimate the cross-spectra $C_{ij}(\ell)$ which should be compatible with zero for the correct choice (similarly to Huterer & White 2005),

or alternatively, one can take advantage of the non-commutativity $[\mathbf{S}, \mathbf{N}] = \mathbf{SN} - \mathbf{NS} \neq 0$ of the signal covariance $\mathbf{S}$ and the noise covariance $\mathbf{N}$. If the polynomials have been constructed for the true cosmology with the first normalization variant equation (23), $\mathbf{S}$ for unit normalized polynomials is equal to the unit matrix and would always commute with $\mathbf{N}$. In the case of the wrong cosmology, $\mathbf{S}$ and $\mathbf{N}$ are symmetric matrices with different eigensystems, and $[\mathbf{S}, \mathbf{N}]$ does not vanish. In Fig. 14 this commutator is given as a function of multipole order ℓ and depending on the number of polynomials used. For giving a single number quantifying the non-commutativity we chose to compute the trace $\mathrm{tr}\,[\mathbf{S}, \mathbf{N}]^2$, because $\mathrm{tr}\,[\mathbf{S}, \mathbf{N}]$ without squaring always vanishes. The stronger systematic (detuning Ω_m and σ_8 from their fiducial values) generates larger values compared to the wrong assumption of a time-varying equation of state of the dark energy component. Naturally, when using a single polynomial $q = 0$ the commutator is always zero.

Given the minor impact on choosing a wrong cosmological impact on parameter estimation from weak lensing spectra weighted with orthogonal polynomials, we point out that it should be possible to employ the polynomials iteratively by alternating between parameter estimation and polynomial construction. At the same time we emphasize the possible usefulness of measuring cross-spectra $C_{ij}(\ell)$, $i \neq j$, or the commutator $\mathrm{tr}\,[\mathbf{S}, \mathbf{N}]^2$ for validating the cosmological model used for data analysis.

6 SUMMARY

The topic of this paper is a novel method of carrying out tomographic weak lensing measurements by line-of-sight weighting of
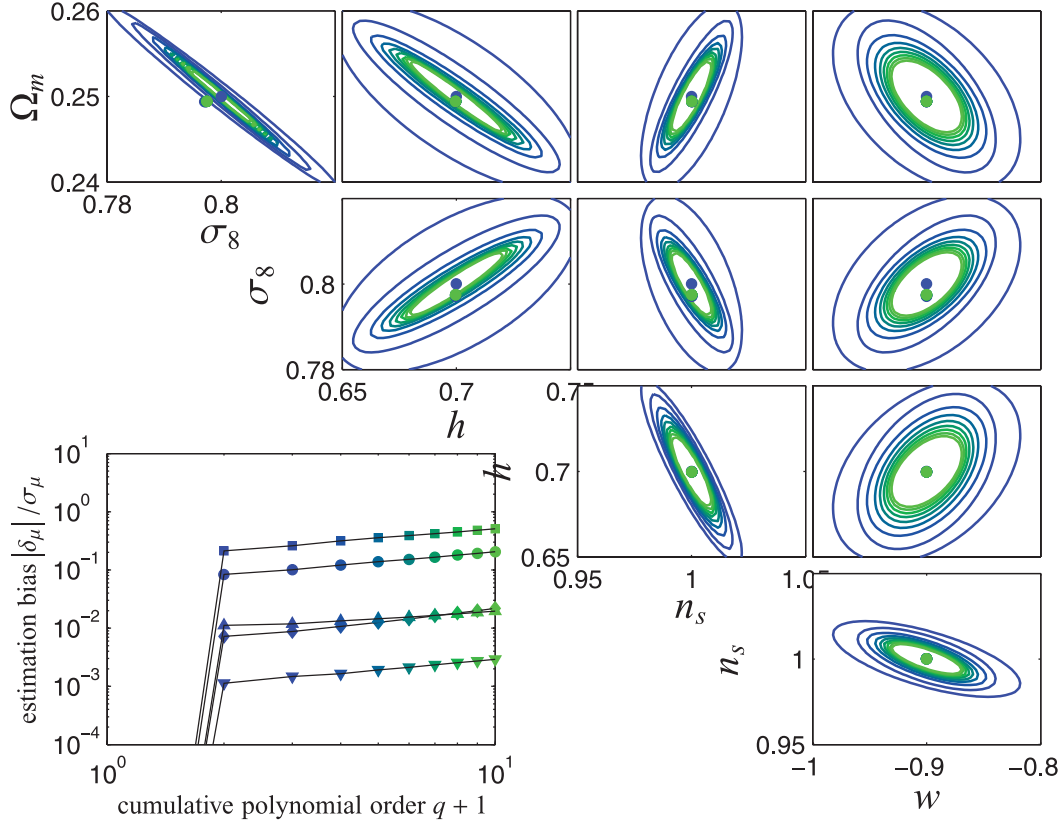
Figure 13. Biases (δ_μ, δ_ν) in the cosmological parameters Ω_m, σ_8, h, n_s and w, superimposed on the 1σ confidence regions, if the true redshift distribution of galaxies differs from the observed one by a convolution with a Gaussian with $\sigma_z = 0.05$. The dot colour changes with cumulative polynomial order q, and is replotted as a function of q in the inset for Ω_m (dots), σ_8 (squares), h (lozenges), n_s (triangles, pointing up) and w (triangles, pointing down). The errors and biases correspond to the *Euclid* survey up to the multipole order $\ell_{max} = 1000$.
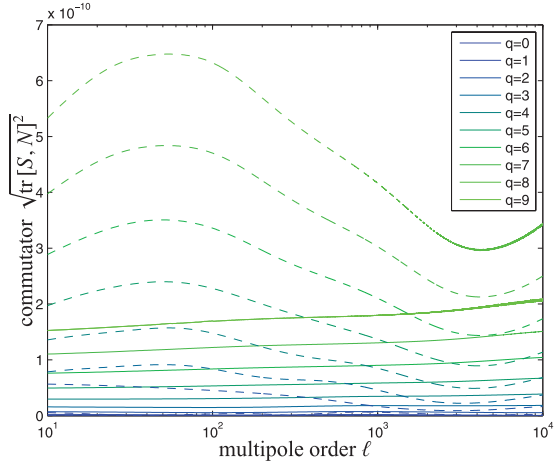
Figure 14. Commutator $\sqrt{\mathrm{tr}\,[\mathbf{S}, \mathbf{N}]^2}$ between the signal covariance S_{ij} and the noise covariance N_{ij}, cumulative in polynomial order q (indicated by colour), for the two systematics considered here: assuming a time-varying instead of a constant wCDM model ($w_0 = -0.8$ and $w_a = -0.2$, solid lines) and choosing a too high matter density and a too high normalization of $P(k)$ ($\Omega_m = 0.275$ and $\sigma_8 = 0.85$, dashed lines), both for *Euclid*.

the weak lensing convergence with specifically constructed orthogonal polynomials.

(i) The TaRDiS polynomials have been constructed with a Gram–Schmidt orthogonalization procedure in order to diagonalize the signal covariance matrix, and to project out statistically independent information of the weak lensing field by performing weak lensing tomography. They differ from traditional tomography and three-dimensional weak lensing methods in the respect that the signal covariance is diagonal instead of the noise covariance.

(ii) The statistical error forecasts for cosmological parameters were investigated with the Fisher matrix formalism. Because of the polynomial's property of providing statistically independent information of the weak convergence field, one sees a particularly simple square-root scaling of the signal-to-noise ratio and the statistical errors with the maximum multipole considered and the number of polynomials used. Our initial hope, namely that a mismatch between the true and the assumed cosmology causes a decrease in likelihood and therefore an increased precision in the determination of cosmological parameter, was not fulfilled. This matching effect, which would cause the Fisher matrix to assume the largest possible values because of the diagonalized covariance would generate the smallest statistical errors. Sadly, this effect is rather weak, which can be as well demonstrated by the small estimation biases if the wrong cosmology is chosen for construction, and does not yield advantages over traditional tomographic methods and would not justify the complexity of constructing polynomials in comparison to straightforward redshift binning.

(iii) We extended the Fisher matrix formalism for investigating how the assumption of a wrong cosmology in the construction of the polynomials impacts on the estimation of cosmological parameters and to what extend biases are introduced. We assumed three systematically wrong priors: assumption of a time varying instead

of a constant dark energy equation of state parameter, as an example of a degree of freedom not contained in the model, a wrong Ω_m- and σ_8 pair, as being the two most prominent parameters determining the strength of the weak lensing signal, and finally a convolved galaxy redshift distribution. All three systematics had a minor impact on the parameter estimation, with the biases decreasing if a larger number of polynomials was used. With 10 polynomials biases were of the order of the statistical error even for strong mismatches in the choice of the initial cosmology. Only the assumption of a wrong redshift distribution generates roughly constant biases, which, when normalized to the statistical errors, increase with the number of polynomials used. Our extension of the Fisher matrix formalism treats the parameter estimation biases in full generality and does not assume a diagonal shape of neither the signal nor the noise covariance.

(iv) The accuracy needed for constructing viable polynomials corresponds to the statistical error reachable with a simple unweighted convergence spectrum, which is readily available, and can be improved by adding additional priors in the form of the CMB likelihood, parameter constraints form baryon acoustic oscillations or from supernovae.

(v) Additionally, it is possible to compute diagnostics for the choice of the prior cosmological model used for constructing the cosmology: examples include the cross-spectra $S_{ij}(\ell)$ for two different polynomials $i \neq j$, which should vanish for correctly constructed polynomials, and the commutator $[\mathbf{S}, \mathbf{N}] = \mathbf{SN} - \mathbf{NS}$ between the signal and the noise covariance, which should vanish if the signal covariance is equal to the unit matrix for a certain choice of normalization for the polynomials.

We plan to extend our research on the usage of orthogonal polynomials to the weak lensing bispectrum in a future paper, and to carry out forecasts on dark energy cosmologies from combined constraints with spectrum and bispectrum tomography.

ACKNOWLEDGMENTS

REFERENCES

Abramowitz M., Stegun I. A., 1972, Handbook of Mathematical Functions. Dover Press, New York
Amara A., Kitching T. D., 2011, MNRAS, 413, 1505
Amara A., Réfrégier A., 2007, MNRAS, 381, 1018
Amara A., Réfrégier A., 2008, MNRAS, 391, 228
Bacon D. J., Refregier A. R., Ellis R. S., 2000, MNRAS, 318, 625
Bardeen J. M., Bond J. R., Kaiser N., Szalay A. S., 1986, ApJ, 304, 15
Bartelmann M., 2010a, Rev. Modern Phys., 82, 331
Bartelmann M., 2010b, Classical Quantum Gravity, 27, 233001
Bartelmann M., Schneider P., 2001, Phys. Rep., 340, 291
Bernstein G., Jain B., 2004, ApJ, 600, 17
Blandford R. D., Saust A. B., Brainerd T. G., Villumsen J. V., 1991, MNRAS, 251, 600
Bridle S., King L., 2007, New J. Phys., 9, 444
Cabré A., Fosalba P., Gaztañaga E., Manera M., 2007, MNRAS, 381, 1347
Carron J., Amara A., Lilly S., 2011, MNRAS, 417, 1938
Castro P. G., Heavens A. F., Kitching T. D., 2005, Phys. Rev. D, 72, 023516
Chevallier M., Polarski D., 2001, Int. J. Modern Phys. D, 10, 213
Hannestad S., Tu H., Wong Y. Y., 2006, J. Cosmol. Astropart. Phys., 6, 25
Heavens A., 2003, MNRAS, 343, 1327
Heavens A. F., Kitching T. D., Taylor A. N., 2006, MNRAS, 373, 105
Hollenstein L., Sapone D., Crittenden R., Schäfer B. M., 2009, J. Cosmol. Astropart. Phys., 4, 12
Hu W., 1999, ApJ, 522, L21
Hu W., 2002a, Phys. Rev. D, 65, 023003
Hu W., 2002b, Phys. Rev. D, 66, 083515
Hu W., Jain B., 2004, Phys. Rev. D, 70, 043009
Hu W., Tegmark M., 1999, ApJ, 514, L65
Hu W., White M., 2001, ApJ, 554, 67
Huterer D., 2002, Phys. Rev. D, 65, 063001
Huterer D., 2010, Gen. Relativ. Gravitation, 42, 2177
Huterer D., Turner M. S., 2001, Phys. Rev. D, 64, 123527
Huterer D., White M., 2005, Phys. Rev. D, 72, 043002
Huterer D., Takada M., Bernstein G., Jain B., 2006, MNRAS, 366, 101
Jain B., Seljak U., 1997, ApJ, 484, 560
Jain B., Taylor A., 2003, Phys. Rev. Lett., 91, 141302
Kaiser N., Wilson G., Luppino G. A., 2000, preprint (astro-ph/000338)
Kamionkowski M., Babul A., Cress C. M., Refregier A., 1998, MNRAS, 301, 1064
Kilbinger M. et al., 2009, A&A, 497, 677
Kilbinger M. et al., 2010, MNRAS, 405, 2381
King L., Schneider P., 2002, A&A, 396, 411
Kitching T. D., Taylor A. N., Heavens A. F., 2008, MNRAS, 389, 173
Kitching T. D., Heavens A. F., Miller L., 2011, MNRAS, 413, 2923
Lee S., 2011, preprint (arXiv:1105.0993)
Limber D. N., 1954, ApJ, 119, 655
Linder E. V., Jenkins A., 2003, MNRAS, 346, 573
Ma Z., Hu W., Huterer D., 2006, ApJ, 636, 21
March M. C., Trotta R., Amendola L., Huterer D., 2011, MNRAS, 415, 143
Refregier A., Amara A., Kitching T. D., Rassat A., 2011, A&A, 528, A33
Schäfer B. M., 2009, Int. J. Modern Phys. D, 18, 173
Schneider P., Ehlers J., Falco E. E., 1992, Gravitational Lenses. Springer-Verlag, Berlin
Seitz S., Schneider P., 1994, A&A, 287, 349
Seitz S., Schneider P., Ehlers J., 1994, Classical Quantum Gravity, 11, 2345
Semboloni E., Hoekstra H., Schaye J., van Daalen M. P., McCarthy I. G., 2011, MNRAS, 417, 2020
Smith R. E. et al., 2003, MNRAS, 341, 1311
Sugiyama N., 1995, ApJS, 100, 281
Taburet N., Aghanim N., Douspis M., Langer M., 2009, MNRAS, 392, 1153
Taburet N., Douspis M., Aghanim N., 2010, MNRAS, 404, 1197
Takada M., Jain B., 2004, MNRAS, 348, 897
Takada M., Jain B., 2009, MNRAS, 395, 2065
Takada M., White M., 2004, ApJ, 601, L1
Taylor A. N., Kitching T. D., Bacon D. J., Heavens A. F., 2007, MNRAS, 374, 1377
Tegmark M., Taylor A. N., Heavens A. F., 1997, ApJ, 480, 22
Turner M. S., White M., 1997, Phys. Rev. D, 56, 4439
Van Waerbeke L. et al., 2000, A&A, 358, 30
Wang L., Steinhardt P. J., 1998, ApJ, 508, 483
Wittman D. M., Tyson J. A., Kirkman D., Dell'Antonio I., Bernstein G., 2000, Nat, 405, 143

APPENDIX A: WEIGHTED LENSING SPECTRA

Fig. A1 provides an alternative representation for Fig. 5 of the polynomial-weighted weak lensing spectra $S_{ii}(\ell)$. Here, the spectra are normalized to the value $S_{00}(\ell = 10^2)$, such that the difference in
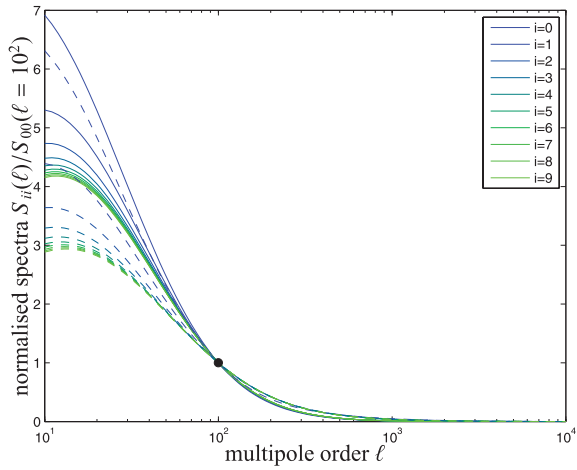
Figure A1. $p_i(\chi)$-weighted weak lensing spectra $S_{ii}(\ell)$, normalized to the value $S_{00}(\ell) \equiv C_\kappa(\ell)$ at $\ell = 10^2$ (indicated by the black dot) for illustrating the change in shape introduced by the polynomials. The weighting polynomials have been constructed for a linear (solid line) and a non-linear (dashed line) CDM spectrum.

shape is easier to see. In particular the low multipoles are suppressed in amplitude by the weighting with $p_i(\chi)$.

This paper has been typeset from a TeX/LaTeX file prepared by the author.